

Higher-Order Virial Coefficients of Water Models

Kenneth M. Benjamin,[†] Jayant K. Singh,[‡] Andrew J. Schultz,[†] and David A. Kofke^{*,†}

Department of Chemical and Biological Engineering, University at Buffalo, The State University of New York, Buffalo, New York 14260-4200, and Department of Chemical Engineering, Indian Institute of Technology, Kanpur, Kanpur, India 208016

Received: February 7, 2007; In Final Form: May 11, 2007

We use the Mayer sampling method, with both direct and overlap sampling, to calculate and compare classical virial coefficients up to B_6 for various water models (SPC, SPC/E, MSPC/E, TIP3P, and TIP4P). The precision of the computed values ranges from 0.1% for B_2 to an average of 25% for B_6 . When expressed in a form scaled by the critical properties, the values of the coefficients for SPC water are observed to greatly exceed the magnitude of corresponding coefficients for the simple Lennard-Jones model. We examine the coefficients in the context of the equation of state and the Joule–Thomson coefficient. Comparisons of these properties are made both to established molecular simulation data for each respective model and to real water. For all models, the virial series up to B_5 describes the equation of state along the saturated vapor line better than the series that includes B_6 . At supercritical temperatures, however, the sixth-order series often describes pressure–volume–temperature behavior better than the fifth-order series. For example, the sixth-order virial equation of state for SPC/E water predicts the 673 K isotherm within 8% of published molecular simulation values up to a density of 9 mol/L (roughly half the critical density of SPC/E water).

1. Introduction

Understanding the pressure–volume–temperature (PVT) behavior of real gases is an active and important research area. It began with van der Waals, who first developed the famous two-constant equation for interpreting real gas behavior.¹ Since then, much work has been done in developing theoretical and empirical methods for predicting and understanding real gas behavior.^{2,3}

In this area, an important role is played by the virial equation of state (VEOS). The VEOS describes the PVT behavior at low density by the following expression,

$$\frac{P}{\rho kT} \equiv Z = 1 + B_2\rho + B_3\rho^2 + B_4\rho^3 + B_5\rho^4 + B_6\rho^5 + \dots \quad (1)$$

where P is the pressure, ρ is the number density (reciprocal of volume per molecule, v), k is the Boltzmann constant, T is the absolute temperature, Z is the compressibility factor, and B_i is the i th virial coefficient. These coefficients are directly related to the interactions between the molecules. The first term on the right-hand side in the above equation (the constant 1) represents the ideal gas contribution, and subsequent terms represent the contributions from many-body interactions as found in real (that is, nonideal) systems. In particular, B_i is related to interaction energies of a group of i molecules. Diagrammatically, these coefficients are represented in the form of cluster integrals.^{2,4} For example

$$B_2(T) = -\frac{1}{2V} \iint f_{12} d\mathbf{r}_1 d\mathbf{r}_2 = -\frac{1}{2V} \text{---} \bullet \text{---} \bullet \quad (2)$$

where V is the volume. For pairwise-additive potentials the third virial coefficient is

$$B_3(T) = -\frac{1}{3V} \iiint f_{12} f_{13} f_{23} d\mathbf{r}_1 d\mathbf{r}_2 d\mathbf{r}_3 = -\frac{1}{3V} \text{---} \triangle \quad (3)$$

In the integrals, $f_{ij} = [\exp(-\beta u_{ij}) - 1]$ is the Mayer function, where u_{ij} is the pair potential between molecules labeled i and j , and $\beta = (kT)^{-1}$. In the diagrams, the points correspond to each variable of integration, and the lines represent Mayer–function interactions between the molecules. The coefficient premultiplying each integral can be determined from a symmetry number associated with the diagram. The integral over one molecule's position cancels the V in the denominator. We write the formulas showing the integration over only the positions of each molecule; in general, integration must be performed over all rotational and internal degrees of freedom available to each molecule, as well. Using now just the diagrammatic form of the integrals, the fourth virial coefficient is

$$B_4(T) = \frac{-1}{8V} \left[3 \text{---} \square \text{---} + 6 \text{---} \square \text{---} + \text{---} \square \text{---} \right] \quad (4)$$

whereas the fifth virial coefficient, $B_5(T)$, is the sum of 10 five-point diagrams.

There are several scientific and engineering uses for virial coefficients. These include

- Testing intermolecular potentials. The temperature dependence of B_2 gives information about the detailed pairwise interactions. Comparison of B_2 for a model to experimental B_2 data provides one means to formulate pairwise potentials. In principle, higher-order virial coefficients also can act as a stringent test for these potentials. However, higher-order virial coefficients are not easily measured experimentally.

- Determining the unknown parameters that appear in approximate equations of state.^{5,6}

* Corresponding author. Tel.: (716) 645-2911 ext. 2215. Fax: (716) 645-3822. E-mail: kofke@buffalo.edu.

[†] The State University of New York.

[‡] Indian Institute of Technology.

TABLE 1: Comparison of Overlap and Direct Sampling for the Calculation of B_2 for TIP4P Water at 298 K^a

sampling method	B_2 (L/mol)	% precision
overlap	-3.639	0.1
direct	-3.324	8.3

^a 10^9 configurations were sampled for each value of B_2 .

- Describing (with virial series up to a few virial coefficients) the supercritical phase during supercritical extraction.^{7,8}
- Predicting PVT behavior, critical properties, and phase instabilities of molecular fluids.^{9,10}
- Predicting the Joule–Thomson inversion curve (from second and third virial coefficients) of molecular fluids.¹¹
- Describing gas-phase molecular clustering.^{12,13}

Despite the diagrammatic simplicity of these virial coefficient expressions, it has been quite difficult to calculate virial coefficients, except for the simplest cases. Some examples of these simpler cases include

- Up to B_{10} for hard spheres in 1–8 dimensional space.^{14,15}
- Up to B_8 for various nonspherical convex hard bodies.¹⁶
- Up to B_5 for particles interacting according to a square-well potential.¹⁶

For more realistic potentials [such as Lennard-Jones fluids (LJ), two-centered LJ with point quadrupoles (2CLJQ), and water], fewer virial coefficients are known. Prior to our recent work, virial coefficients up to only B_5 for LJ,¹⁷ B_4 for 2CLJQ,¹⁰ and B_3 for water⁹ have been determined using the existing methodologies, that is, numerical integration⁹ and the hit-and-miss Monte Carlo (MC) method.¹⁸ Rouha and Nezbeda have reported B_2 and B_3 for some primitive models of polar and associating fluids.¹⁹ Recently, we proposed Mayer sampling, a method based on free energy perturbation ideas applied to the calculation of cluster integrals.²⁰ We demonstrated the effectiveness of this method by calculating up to B_6 for LJ and B_5 for the SPC/E water model.²⁰

In the present study, we apply the Mayer sampling method to calculate up to B_6 for various pairwise water models; specifically, SPC, SPC/E, MSPC/E, TIP3P, and TIP4P.^{21–25} We also investigate the PVT behavior of these models on the basis of successive truncated virial series. All calculations described herein are classical and contain no quantum mechanical corrections, even though such effects are known to be significant at some of the conditions studied here.²⁶ For example, in the case of the TIP4P water model, quantum effects can alter B_2 by 60% at 350 K. The effects diminish with increasing temperature and at 500 K are negligible. Regardless, it is worth keeping in mind that some empiricism was used in the development of these classical models, and consequently, their formulation implicitly includes quantum effects to some degree (much as they also attempt to capture the effect of multibody interactions in the parametrization of their pairwise form). Quantum effects become increasingly important at low temperatures, and their neglect is likely to lead to significant errors when extrapolating to temperatures below those used to fit the models.

The rest of the paper is organized as follows. In the next section, we review the Mayer sampling technique. In Section 3, we present the results for the water models and also discuss thermodynamic properties predicted from the truncated series. Finally, we conclude in Section 4.

2. Molecular Models and the Mayer Sampling Method

This section outlines the specific water models studied and the Mayer sampling method itself. Particular attention is drawn

to two different staging schemes used in this work: direct sampling and overlap sampling.

2.1. Molecular Models for Water. In this investigation, we apply the Mayer sampling method to calculate values of B_2 – B_6 for various pairwise water models; specifically, SPC, SPC/E, MSPC/E, TIP3P, and TIP4P.^{21–25} These simple models, especially SPC/E and TIP4P, are often considered the best pairwise models available for water and have received much attention in the molecular simulation literature for studying such phenomena as vapor–liquid equilibrium, thermodynamic properties, transport properties, and solvation.

2.2. Direct Sampling. Mayer sampling²⁰ is based on importance-sampling Metropolis Monte Carlo simulation to evaluate each n -point cluster integral or, more generally, sums of such integrals. It is similar in nature to other biased Monte Carlo methods for evaluating cluster integrals.^{27–30} A probability distribution $\pi(\mathbf{r}^n)$ governs sampling of configurations, and simulation is used to evaluate the ratio of each integral to a known reference integral. This is represented mathematically as

$$\Gamma(T) = \Gamma_0 \frac{\Gamma}{\Gamma_0} = \Gamma_0 \frac{\langle \gamma / \pi \rangle_\pi}{\langle \gamma_0 / \pi \rangle_\pi} \quad (5)$$

In the above expression, $\Gamma(T)$ represents a general cluster integral or sum of integrals with integrand $\gamma(\mathbf{r}^n; T)$. For example, if Γ is B_3 , then $\gamma \equiv f_{12}f_{13}f_{23}$, and if Γ is B_4 , then $\gamma = (3)f_{12}f_{23}f_{34}f_{14} + (6)f_{12}f_{23}f_{34}f_{14}f_{13} + f_{12}f_{23}f_{34}f_{14}f_{13}f_{24}$. The angle brackets indicate the “ensemble-average” integral over all configurations and orientations of the n molecules, and the subscript π indicates that the integral is weighted by the (normalized) π distribution: $\langle M \rangle_\pi \equiv \int d\mathbf{r}^n M \pi / \int d\mathbf{r}^n \pi$. The subscript “0” indicates a quantity for a reference system, for which Γ_0 is known. Although superficially of the form of umbrella sampling, we refer to eq 5 as the direct-sampling implementation of Mayer sampling because it involves perturbations directly between the target system (which governs sampling) and the reference system.³¹ This approach was used to calculate all of the virial coefficients (B_2 – B_5) reported here for all of the water models, with the exception of B_5 for SPC/E water at all temperatures and B_2 – B_5 for TIP4P water at temperatures between 210 and 298 K. In those instances and for all values of B_6 for all water models, the overlap sampling scheme was used. More information on overlap sampling can be found in the following subsection.

There are many choices one can select for the π distribution and reference cluster.²⁰ In this work, we have used $\pi = |\gamma(\mathbf{r}^n; T)|$, as suggested by the importance sampling approach. We have found that selecting π as the absolute value of the sum of all the clusters is a convenient formulation. By choosing this definition for π , eq 5 can be expressed as

$$\Gamma(T) = \Gamma_0 \frac{\langle \text{sgn}(\gamma) \rangle_\pi}{\langle \gamma_0 / \pi \rangle_\pi} \quad (6)$$

where $\text{sgn}(\gamma)$ is just the sign of the cluster sum. Therefore, each term in the numerator average is +1 or -1.

Regarding the reference cluster, one must select a system whose phase space is a subset of the phase space of the target system.^{32,33} In this work, we used the ring-shaped cluster with a hard-sphere potential as a reference for all of our direct sampling simulations, and the sum of all diagrams and a hard-sphere potential as a reference for all overlap sampling simulations. Other choices are possible. Although the hard-sphere potential and the water potentials are very different, the impact

TABLE 2: Virial Coefficients for the SPC/E Model of Water²² as Calculated Using the Mayer Sampling Method^a

T (K)	B_2^b (L/mol)	B_3^b (L/mol) ²	B_4^b (L/mol) ³	B_5^c (L/mol) ⁴	B_6^c (L/mol) ⁵
373	-1.8049(4)	-10.29(8)	-243(20)	577(14)	$1.50(45) \times 10^4$
423	-0.8865(4)	-1.045(2)	-2.85(10)	15.2(2)	16.7(3)
450	-0.65288(8)	-0.3479(8)	-0.256(13)	2.243(33)	-0.46(23)
473	-0.5189(1)	-0.1373(3)	0.0335(10)	0.524(9)	-0.472(43)
500	-0.4082(2)	-0.04106(9)	0.0498(7)	0.0954(21)	-0.102(13)
523	-0.33954(4)	-0.00874(6)	0.0337(4)	0.0213(7)	-0.028(2)
550	-0.2788(1)	0.00623(4)	0.0189(3)	0.0022(2)	-0.00856(68)
573	-0.2391(1)	0.01076(1)	0.0112(3)	-0.00084(11)	-0.0017(3)
600	-0.2024(1)	0.012047(9)	0.0061(1)	-0.00112(5)	-0.00059(11)
623	-0.17715(4)	0.01165(1)	0.00358(3)	-0.00092(2)	-0.00021(6)
650	-0.15302(9)	0.010582(5)	0.00195(2)	-0.000635(18)	-0.00005(1)
673	-0.13599(2)	0.009530(6)	0.00115(1)	-0.00040(1)	0.00003(3)
700	-0.1192(52)	0.008318(3)	0.000636(7)	-0.000258(7)	0.000084(70)
723	-0.10714(20)	0.007380(3)	0.000377(5)	-0.000184(6)	0.000021(10)
750	-0.09493(5)	0.006392(1)	0.000188(5)	-0.000121(3)	0.0000065(17)
773	-0.08596(5)	0.005674(3)	0.000095(2)	-0.000082(2)	0.000010(2)

^a Numbers in parentheses represent the confidence limits (standard error of the mean) for the rightmost digits of the value. ^b Values for B_2 , B_3 , and B_4 are determined from direct sampling. ^c Values for coefficients B_5 and B_6 were determined in this investigation using overlap sampling, with at least 10^8 configurations sampled for each coefficient.

TABLE 3: Virial Coefficients for the SPC Model of Water²¹ as Calculated Using the Mayer Sampling Method^a

T (K)	B_2^b (L/mol)	B_3^b (L/mol) ²	B_4^b (L/mol) ³	B_5^b (L/mol) ⁴	B_6^c (L/mol) ⁵
350	-1.632(1)	-7.43(5)	-110(8)	475(86)	$5.49(72) \times 10^3$
370	-1.1856(1)	-2.66(1)	-17(2)	149(34)	338(25)
390	-0.8963(3)	-1.053(5)	-3.1(1)	24(5)	14(3)
410	-0.7003(2)	-0.436(2)	-0.40(1)	4.6(4)	-0.2(3)
430	-0.5605(2)	-0.1826(4)	-0.001(3)	0.9(2)	-0.57(5)
450	-0.4590(3)	-0.0732(2)	0.057(1)	0.20(2)	-0.228(6)
470	-0.3826(2)	-0.0242(1)	0.045(1)	0.057(7)	-0.0702(27)
490	-0.32393(4)	-0.00242(3)	0.0291(2)	0.012(1)	-0.025(1)
510	-0.27779(3)	0.00726(3)	0.0180(1)	0.0017(1)	-0.0082(6)
530	-0.24065(7)	0.01113(3)	0.0110(1)	-0.00098(3)	-0.0027(1)
550	-0.2106(2)	0.01226(3)	0.00674(4)	-0.00124(2)	-0.00106(6)
570	-0.1856(1)	0.01206(1)	0.00415(3)	-0.00109(5)	-0.00034(6)
590	-0.16466(9)	0.01130(1)	0.00256(1)	-0.00076(1)	-0.000085(17)
610	-0.14717(6)	0.01033(1)	0.00161(1)	-0.00055(1)	-0.000016(11)
630	-0.13196(5)	0.009302(3)	0.000992(4)	-0.00038(1)	0.000019(7)
650	-0.1191(2)	0.008331(4)	0.000608(5)	-0.000253(3)	0.000012(4)
670	-0.10777(9)	0.007448(5)	0.000366(6)	-0.000182(3)	0.0000074(43)
690	-0.09796(6)	0.006647(4)	0.000214(2)	-0.000132(2)	0.000015(2)
710	-0.0891(1)	0.005934(3)	0.000118(2)	-0.000089(2)	0.000010(1)
730	-0.08142(4)	0.005315(2)	0.000050(1)	-0.000066(2)	0.0000078(14)
750	-0.07455(7)	0.004768(2)	0.000016(1)	-0.000047(2)	0.0000076(18)

^a Numbers in parentheses represent the confidence limits (standard error of the mean) for the rightmost digits of the value. ^b Values for B_2 , B_3 , B_4 , and B_5 are determined from direct sampling. ^c Values for B_6 were determined in this investigation using overlap sampling, with at least 10^8 configurations sampled for each coefficient.

of this difference on the accuracy and precision of the calculations is minimal so long as the sampling method can sample configurations important to both systems.

The calculations were conducted as follows. Monte Carlo sampling was performed for a number of molecules equal to the order of the virial coefficient being computed. We used molecule displacement and rotation moves to generate trial configurations. We found it helpful to select a random number of molecules to perturb in one trial (so, e.g., with equal likelihood, sometimes one molecule is moved, sometimes two, etc., and sometimes all of them are). Each trial was accepted with probability $\min(1, \pi^{\text{new}}/\pi^{\text{old}})$, where π is defined as the absolute value of the weighted sum of the cluster integrands contributing to the calculated virial coefficient. The resulting configuration contributed to the two averages in eq 6. We examined several values of the reference hard-sphere diameter near the LJ collision diameter σ (for the oxygen atom in the water models) and did not observe a significant effect on the results. The value of a cluster for a given configuration was determined by summing the contributions of all unique permutations of the labeling of the molecules. Simulations sampled

$M = 10^7-10^9$ configurations, depending on the rate of convergence of the averages. Step sizes for the trials were adjusted in a short "equilibration" period, before accumulating averages, to achieve a 50% acceptance rate for trial moves. It is important that this step size not be adjusted once averaging is begun.

Virial coefficients up to B_4 for the water models are easily done on a single processor in 3 days or less. For higher-order coefficients (B_5 and B_6), longer runs are required to collect the required number of configurations. Hence, parallelization is a very valuable feature of the current method. Multiprocessors were utilized for calculating higher-order virial coefficients. For example, calculating B_6 at a given temperature required 12 h on 128 3.2 GHz processors. The independent averages were collected and processed at the end of the simulation to calculate the desired virial coefficient. All simulations in this work were performed with the etomica molecular simulation suite.³⁴ We note that it is likely that the present implementation is not the most optimized form and believe that further advancement in the algorithm will lead to the improvement in the efficiency of the method.

TABLE 4: Virial Coefficients for the MSPC/E Model of Water²³ as Calculated Using the Mayer Sampling Method^a

T (K)	B_2 (L/mol)	B_3 (L/mol) ²	B_4 (L/mol) ³	B_5 (L/mol) ⁴	B_6 (L/mol) ⁵
350	-1.922(2)	-13.05(10)	$-4(1) \times 10^2$	$4(1) \times 10^3$	$3.15(60) \times 10^4$
370	-1.368(2)	-4.61(2)	-45(4)	$6(1) \times 10^2$	$1.59(16) \times 10^3$
390	-1.017(1)	-1.787(3)	-7.2(8)	72(10)	102(10)
410	-0.7841(4)	-0.727(4)	-1.55(5)	6.9(7)	7.01(83)
430	-0.6201(4)	-0.3110(5)	-0.185(7)	2.4(3)	-0.278(94)
450	-0.5027(3)	-0.1339(3)	0.0245(6)	0.55(6)	-0.34(1)
470	-0.4155(2)	-0.05435(8)	0.046(2)	0.12(1)	-0.128(6)
490	-0.3493(2)	-0.01766(9)	0.0352(4)	0.024(3)	-0.0466(28)
510	-0.2977(8)	-0.00065(3)	0.0234(2)	0.0090(3)	-0.0154(6)
530	-0.2564(2)	0.00693(2)	0.0143(2)	0.00108(4)	-0.0045(3)
550	-0.2236(2)	0.01003(1)	0.00897(4)	-0.00055(3)	-0.0021(1)
570	-0.1963(1)	0.01087(2)	0.00557(9)	-0.00098(7)	-0.00068(5)
590	-0.1737(2)	0.01070(2)	0.00346(3)	-0.00086(1)	-0.00032(7)
610	-0.1546(1)	0.010038(6)	0.00218(1)	-0.000576(8)	-0.00006(3)
630	-0.1388(1)	0.009192(7)	0.001367(6)	-0.000434(7)	-0.00002(2)
650	-0.1247(1)	0.008325(6)	0.000862(8)	-0.000299(2)	0.000002(11)
670	-0.11287(9)	0.007484(4)	0.000528(4)	-0.000221(2)	0.0000098(41)
690	-0.10233(7)	0.006705(6)	0.000324(1)	-0.000155(1)	0.000016(2)
710	-0.0931(2)	0.006007(5)	0.000193(3)	-0.000110(1)	0.000014(3)
730	-0.08497(6)	0.005381(3)	0.000107(1)	-0.000075(1)	0.000006(2)
750	-0.07771(7)	0.004832(3)	0.000052(1)	-0.000055(3)	0.000006(1)

^a See Table 3 footnotes *a-c*.**TABLE 5: Virial Coefficients for the TIP3P Model of Water²⁴ as Calculated Using the Mayer Sampling Method^a**

T (K)	B_2 (L/mol)	B_3 (L/mol) ²	B_4 (L/mol) ³	B_5 (L/mol) ⁴	B_6 (L/mol) ⁵
350	-1.657(2)	-6.57(2)	-99(6)	186(72)	$6.23(47) \times 10^3$
370	-1.211(1)	-2.45(1)	-16(3)	64(13)	373(31)
390	-0.9207(6)	-0.988(3)	-2.64(2)	14(5)	34(4)
410	-0.7217(5)	-0.415(1)	-0.42(2)	3.6(9)	1.9(4)
430	-0.5799(58)	-0.1759(4)	-0.0019(5)	0.94(9)	-0.14(7)
450	-0.4760(2)	-0.0703(1)	0.056(1)	0.19(2)	-0.15(2)
470	-0.3981(2)	-0.02252(7)	0.0466(9)	0.062(8)	-0.0603(41)
490	-0.3374(2)	-0.00083(8)	0.0319(5)	0.018(3)	-0.029(1)
510	-0.2901(2)	0.00882(3)	0.0206(2)	0.0035(2)	-0.0108(5)
530	-0.2505(42)	0.01262(3)	0.01291(8)	-0.0006(1)	-0.0042(5)
550	-0.2218(37)	0.01359(1)	0.00794(4)	-0.0012(1)	-0.00171(6)
570	-0.1947(1)	0.01335(1)	0.00499(2)	-0.00106(3)	-0.0006(1)
590	-0.1732(2)	0.012466(6)	0.00315(2)	-0.00081(4)	-0.00015(5)
610	-0.1547(2)	0.011384(4)	0.00202(2)	-0.00064(2)	-0.00008(1)
630	-0.1390(1)	0.010287(6)	0.001286(5)	-0.000468(8)	-0.000008(9)
650	-0.1255(2)	0.009227(5)	0.000828(4)	-0.00031(1)	0.000015(7)
670	-0.1137(2)	0.008242(6)	0.000510(5)	-0.000232(6)	0.0000202(23)
690	-0.1035(2)	0.007369(4)	0.000323(3)	-0.000165(3)	0.000018(4)
710	-0.09436(9)	0.006593(4)	0.000189(3)	-0.000122(1)	0.0000094(27)
730	-0.08625(9)	0.005909(4)	0.000109(1)	-0.000093(5)	0.000013(2)
750	-0.07907(8)	0.005303(2)	0.000055(2)	-0.000067(1)	0.000007(2)

^a See Table 3 footnotes *a-c*.

2.3. Overlap Sampling. Direct sampling was used to calculate most of the virial coefficients reported in this study. However, for B_5 for SPC/E water at all temperatures, B_6 for all water models at all temperatures, and B_2 – B_6 for TIP4P water from 210 to 298 K, we used overlap sampling instead.¹³ In general, overlap sampling is an alternative free-energy-perturbation technique for sampling systems having overlapping but nonsubset important configurations.^{32,33} The main idea is to sample two separate systems, with each perturbing into a common intermediate. This intermediate is designed to contain important configurations from the intersection of the individual configurations of the two original systems. Bennett developed a method to optimize this intermediate to balance the contributions from the target and reference systems to the overlapping phase space.^{35,36}

Overlap sampling is a desirable alternative to direct sampling at low temperature. At low temperatures, the water molecules strongly prefer their own energetic wells, and many configura-

tions important to the hard sphere reference are not sampled and direct sampling fails. This signals that the hard sphere phase space is no longer a subset of the water phase space,^{32,33} but instead, that the water's attractive wells are regions of phase space overlap between the hard spheres and water. Overlap sampling takes advantage of this overlap by simulating two systems, one with the sampling governed by the water potential and the other governed by the hard sphere potential. One begins by defining an overlap function to represent mathematically only those regions important to both hard spheres and water,

$$\gamma_{os} = \frac{|\gamma_{ol}||\gamma|}{\alpha|\gamma_{ol}| + |\gamma|} \quad (7)$$

where γ_{os} is the overlap function and α is an optimization parameter. In each phase, the quantity measured during the simulation is the ratio of the average value of the cluster to the average overlap function for that system. The ratio of the water

TABLE 6: Virial Coefficients for the TIP4P Model of Water²⁵ as Calculated Using the Mayer Sampling Method^{a,b}

T (K)	B_2 (L/mol)	B_3 (L/mol) ²	B_4 (L/mol) ³	B_5 (L/mol) ⁴	B_6 (L/mol) ⁵
210	-92.76(8)	-1.058(36) × 10 ⁶	-2.64(71) × 10 ⁹	-3.76(89) × 10 ⁹	-2(1) × 10 ⁵
230	-34.11(3)	-5.97(15) × 10 ⁴	-4.16(98) × 10 ⁸		
250	-15.14(1)	-5.85(11) × 10 ³	-1.08(12) × 10 ⁷	-4.25(80) × 10 ⁸	-1.48(84) × 10 ⁵
270	-7.738(6)	-888(13)	-3.87(23) × 10 ⁵	-1.54(13) × 10 ⁷	
290	-4.438(3)	-173(2)	-2.32(9) × 10 ⁴	-1.96(8) × 10 ⁵	
298	-3.639(3)	-93(1)	-8.25(31) × 10 ³	3.50(7) × 10 ⁴	-4(2) × 10 ⁵
350	-1.315(2)	-4.06(4)	-32(3)	170(74)	359(40)
370	-0.9752(8)	-1.52(1)	-5.2(3)	47(5)	12(3)
390	-0.7483(4)	-0.605(2)	-0.64(3)	3.1(2)	-1.33(31)
410	-0.592(3)	-0.2467(8)	-0.015(2)	1.30(7)	-0.8(1)
430	-0.4797(2)	-0.0981(3)	0.0597(2)	0.16(3)	-0.264(17)
450	-0.3961(2)	-0.0341(1)	0.0496(6)	0.051(2)	-0.082(4)
470	-0.3328(2)	-0.00628(7)	0.0308(3)	0.0090(4)	-0.0182(13)
490	-0.2832(2)	0.00589(5)	0.0184(2)	0.00016(9)	-0.00786(63)
510	-0.2443(2)	0.01067(4)	0.01096(7)	-0.00155(5)	-0.0021(3)
530	-0.2124(3)	0.01211(3)	0.00644(4)	-0.00149(3)	-0.000586(95)
550	-0.1865(2)	0.01199(2)	0.00382(3)	-0.00110(2)	-0.00018(3)
570	-0.1647(1)	0.01126(2)	0.00226(2)	-0.00073(1)	-0.00004(2)
590	-0.1467(1)	0.01025(1)	0.001326(9)	-0.000514(6)	0.000005(11)
610	-0.1313(1)	0.00920(1)	0.000786(6)	-0.000337(3)	0.000024(9)
630	-0.1178(1)	0.00819(1)	0.000436(4)	-0.000229(2)	0.000017(5)
650	-0.1065(1)	0.00728(1)	0.000239(3)	-0.000154(2)	0.000016(4)
670	-0.0962(15)	0.006467(5)	0.000112(2)	-0.000105(1)	0.000011(3)
690	-0.0877(1)	0.005749(4)	0.000039(2)	-0.0000723(7)	0.000010(2)
710	-0.0797(1)	0.005123(4)	-0.000018(9)	-0.0000499(5)	0.0000074(12)
730	-0.0728(1)	0.004573(3)	-0.000031(1)	-0.0000357(4)	0.000006(1)
750	-0.0668(1)	0.004098(3)	-0.000047(1)	-0.0000256(3)	0.0000030(5)

^a Numbers in parentheses represent the confidence limits (standard error of the mean) for the rightmost digits of the value. ^b All coefficients from 210 to 298 K as well as values for B_6 at all temperatures were determined in this investigation using overlap sampling, with at least 10⁸ configurations sampled for each coefficient. Values at all other temperatures are determined from direct sampling.

to the hard sphere integrals can then be calculated as the ratio of the ratios from the hard sphere and water systems,

$$\Gamma(T) = \Gamma_0 \frac{\langle \gamma/\pi \rangle_\pi / \langle \gamma_{OS}/\pi \rangle_\pi}{\langle \gamma_0/\pi_0 \rangle_{\pi_0} / \langle \gamma_{OS}/\pi_0 \rangle_{\pi_0}} \quad (8)$$

where $\pi_0 = |\gamma_0|$.

The important component in overlap sampling is α , the optimization parameter. As a starting point, Bennett^{35,36} developed the following criterion for optimizing α ,

$$\sum_r \gamma_{OS}/\pi_0 = \alpha \sum_t \gamma_{OS}/\pi \quad (9)$$

where the subscripts “r” and “t” refer to the reference and target systems, respectively, and the summations are performed over all the samples in each respective system. However, the criterion in eq 9 assumes that the statistical uncertainties for both systems are equal for the same number of samples. This assumption is not valid for Mayer sampling between a reference system of hard spheres and a target system of water; the water system is much more difficult to sample and therefore contains greater statistical uncertainty. However, if one samples the target system more than the reference system, the value of α from eq 9 becomes smaller. Subsequently, a smaller value of α increases the statistical uncertainty in $\langle \gamma_{OS}/\pi \rangle_\pi$, which in turn increases the statistical uncertainty in $\Gamma(T)$ according to eq 8. Therefore, we require a modified criterion so that we can simulate the target system (water) more than the reference system without biasing the optimal value of α . A more general form of eq 9 is

$$\langle \gamma_{OS}/\pi_0 \rangle_{\pi_0} = \alpha \langle \gamma_{OS}/\pi \rangle_\pi \quad (10)$$

Equation 10 is equivalent to eq 9 if the number of samples for the reference and target systems is the same and will still yield the same value of α when the target system is sampled

more than the reference. We use the statistical uncertainty of the result from each simulation (of each system) to help us choose how long to run each simulation (of each system). On average, the hard sphere reference system is simulated 100 times less than the target (water) system. Ultimately, this methodology allows us to reduce the error in $\Gamma(T)$ as determined by propagation of error on eq 8.

The overlap sampling calculations were conducted in much the same way as the direct sampling calculations, except that we used two systems. One was sampled according to π_0 (the probability distribution for the reference system) and yielded the average for the denominator in eq 8. The second was sampled according to π (the probability distribution for the target system) and yielded the average for the numerator in eq 8.

It is instructive to examine the difference that overlap sampling makes at low temperatures for TIP4P water in Mayer sampling. Table 1 shows the results for B_2 at 298 K calculated with both direct and overlap sampling for 10⁹ configurations. These results clearly show that using overlap sampling at low temperatures improves the precision of the computed value for B_2 . With this level of improvement for B_2 , it is likely that overlap sampling will improve the precision for the higher virial coefficients, B_3 – B_6 , as well. This improvement in precision was realized for B_5 and B_6 for SPC/E water, which were determined with both direct and overlap sampling. The overlap sampling results were more precise, and those values are reported in this work. All Mayer sampling simulations with overlap sampling sampled between 10⁸ and 10¹⁰ configurations (total for both reference and target systems) for each virial coefficient.

We conclude this section with a word on uncertainty analysis. For B_2 , B_3 , and B_4 , about four simulations with 10⁸–10⁹ samples was required to obtain a low uncertainty (usually $\leq 2\%$, except for B_4 at low temperatures). For the higher-order coefficients B_5 and B_6 , typically 8–10 independent simulations of 10⁹ configurations were performed for each coefficient. From these

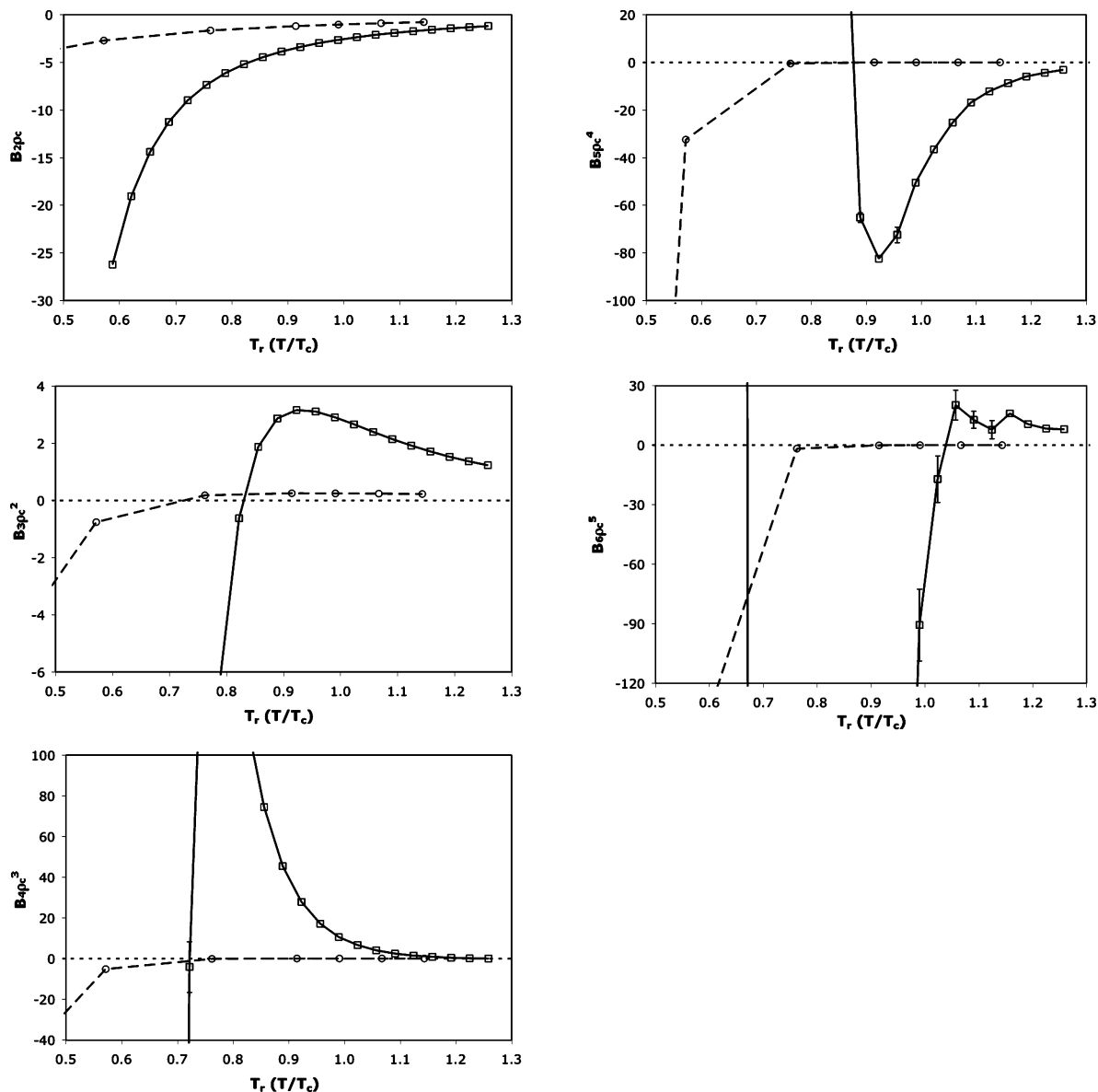


Figure 1. Virial coefficients B_2 – B_6 for the Lennard-Jones model (circles, dashed line) and for the SPC model of water (squares, solid line). Values are made dimensionless by the appropriate power of the critical density, ρ_c , of each model: specifically, 0.289 g/mL for SPC water²³ and 0.31/ σ^3 for the LJ fluid.⁴⁶ T_c is the critical temperature, which equals 596 K for SPC water²¹ and 1.313(ϵ/k_B) for the LJ fluid⁴⁶ (where ϵ is the LJ energy parameter and k_B is Boltzmann's constant). Lines connecting points are drawn as a guide to the eye. The nearly vertical lines in the plots for B_4 and B_6 near $T_r = 0.7$ connect off-of-scale points for SPC water.

independent simulations for each coefficient at each temperature, an average and standard error of the mean for each coefficient was computed and is reported with the results.

3. Results and Discussion

Tables 2–6 present the virial coefficients B_2 – B_6 for all of the water models studied in this work, and Figure 1 presents the coefficients for SPC water in comparison to values for the LJ model (for the purposes of this comparison, we take the SPC data as representative of all water models). To promote a more meaningful comparison of the coefficients between the LJ and water models, in this figure, all values are reduced by the corresponding critical-point properties for each model. From the figure, we see that the virial coefficients for the water model differ quantitatively and sometimes qualitatively from the LJ behavior. Over the range of temperature studied here, the coefficients B_2 , B_3 , and B_4 for the two models follow similar trends, varying from negative to positive values with increasing

temperature. However the scaled magnitudes of the coefficients are very different for the two models: the coefficients for water are many times larger in magnitude than those for the LJ model. This disparity is present even more in the next two coefficients, B_5 and B_6 , which further exhibit qualitative differences between models. For LJ,²⁰ B_5 is negative at low temperatures and increases toward zero with increasing temperature, showing small and brief oscillation there (not visible in figure) as the temperature is increased further, before finally settling in on positive values at high temperature. In contrast, at low temperature (within the range studied) B_5 for water is positive, and with increasing temperature, it drops toward zero, becomes negative, and goes through a steep minimum before returning toward zero (remaining negative) at higher temperatures.

The behavior of B_6 for water is a little harder to generalize. Its value for all models becomes positive at high temperatures. However, at the lower temperatures studied here, B_6 can exhibit either positive or negative values, depending on the particular

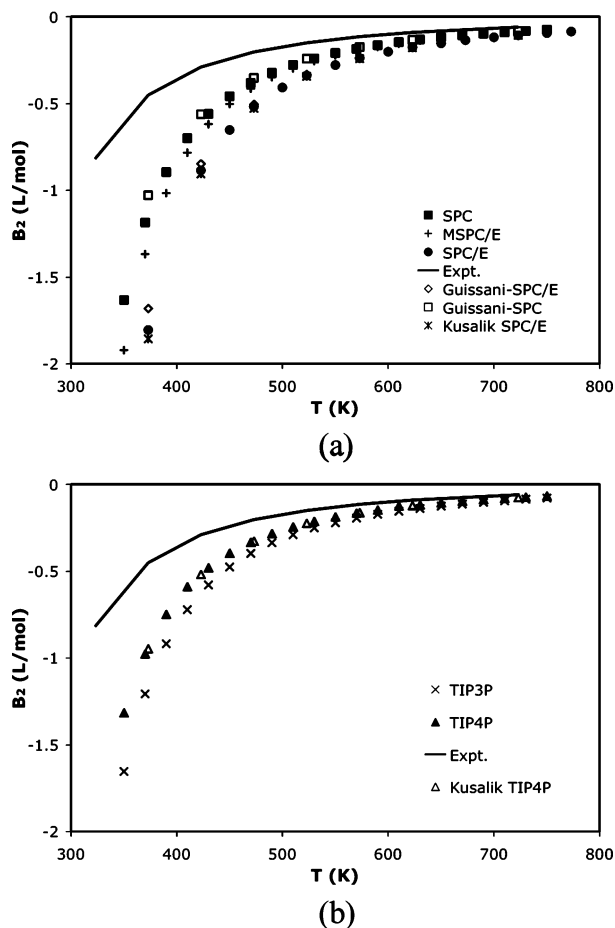


Figure 2. Comparison of second virial coefficient from various water models. Points are Mayer sampling results for each corresponding model or data from the studies by Guissani and Guillot³⁷ and Kusalik et al.⁹ (a) SPC, SPC/E, and MSPC/E. (b) TIP3P and TIP4P. The line labeled “Expt.” represents the correlation given in ref 38.

water model. For SPC water, B_6 proceeds from large and positive at low temperatures to negative at intermediate temperatures and, finally, to small and positive at high temperatures. It seems to show some oscillation above zero at the higher temperatures, and this feature is seen in several of the water models. In contrast, B_6 for the LJ fluid simply proceeds gradually from negative values at low temperatures to small and positive values at higher temperatures.

The data in Tables 2–6 provide for some general observations about the behavior of the virial coefficients across the different water models:

- Of all the water models, TIP4P consistently exhibits the most negative values for B_2 – B_6 .
- As a whole, SPC/E water produces the largest, most positive values for B_2 – B_6 .
- MSPC/E typically yields larger values for B_2 – B_6 than SPC water, but in the cases of B_2 , B_3 , and B_5 , the values get closer to SPC values at higher temperatures.
- TIP3P, like MSPC/E, produces values for B_2 – B_6 that are larger than SPC water, but its values usually are closer to those of SPC water than those belonging to MSPC/E. Some exceptions include B_2 and B_4 , where TIP3P values diverge from SPC values at high temperatures.

Figure 2a–b presents a comparison of second virial coefficients from each water model. The behavior for all models is similar across the temperature range considered in this study. Overall, the agreement between the models is better at high

TABLE 7: Values for B_3 from TIP4P Water Model, Comparing Mayer Sampling Values to Values Obtained from the Literature

T (K)	B_3 (L/mol) ² ; TIP4P, lit. ⁹	B_3 (L/mol) ² ; TIP4P, Mayer sampling ^{a,b}
373	−1.29	−1.35
423	−0.1286	−0.1405
473	−0.001375	−0.00398
523	0.01275	0.01178
573	0.0115	0.01110
623	0.00876	0.00853
673	0.00648	0.006350
723	0.00483	0.004760
773	0.00367	<i>c</i>

^a Values are from interpolation. ^b Values are present with all significant digits, assuming there are no errors introduced from interpolation. ^c 773 K lies outside the temperature range where Mayer sampling values for TIP4P have been determined.

temperature and worse at low temperature. For example, at 750 K, B_2 from the SPC/E model is 42% larger than B_2 from the TIP4P model, but at 450 K, B_2 from the SPC/E model is 65% larger than B_2 from the TIP4P model. This difference is attributed wholly to the water model itself, because the error in the Mayer sampling method is significantly less than 1% for a B_2 calculation. We also compare values calculated via Mayer sampling with the literature value of some models (SPC, SPC/E, and TIP4P). Our values agree well with those from Kusalik et al.⁹ and Guissani and Guillot³⁷ for TIP4P-SPC/E and SPC/E-SPC water models, respectively. It should also be noted that the B_2 values of TIP4P are closest to the values from a high-accuracy correlation for real water,³⁸ whereas B_2 values of SPC/E are farthest. In general, all the pairwise water models investigated significantly underpredict (that is, are more negative than) the actual value of B_2 for water because all the water models were designed to describe condensed (mainly liquid) water, for which the molecular dipole moment is larger and interactions are stronger.

Last, Table 7 presents the results for B_3 TIP4P water calculated from Mayer sampling in comparison to those determined by Kusalik et al.⁹ These data supplement a similar comparison presented previously²⁰ for the SPC/E model. It should be noted that the Mayer sampling values for TIP4P displayed in Table 7 are not directly from simulation but, rather, are interpolations from the values obtained and presented in Table 6. We interpolate using second-order polynomial curves between successive data points. Overall, the values from both studies are largely in agreement: except for where the value is going through zero, differences are <10% and, most often, just a few percent. Interpolation errors notwithstanding, the values obtained from this Mayer sampling investigation are more precise than those previously reported (1% precision from Mayer sampling, 10% precision from Kusalik et al.).

3.1. Thermodynamic Properties. In this section, we consider thermodynamic properties calculated from the virial series of the different water models. The properties we are most interested in are deviations from ideality at saturated vapor conditions and supercritical conditions and Joule–Thomson coefficients.

3.1.1. Prediction of PVT Behavior of Saturated Vapor and Supercritical Conditions. We examine the ability of different truncated virial EOSs to predict the PVT behavior of the corresponding water model. To explore this topic, we focus our attention on PVT behavior at subcritical temperatures along the saturated vapor line, as well as at supercritical temperatures. We compare the predictions of fifth- and sixth-order truncated virial equations of state (denoted VEOS5 and VEOS6, respectively) with molecular simulation data in the literature.^{23,37,39} It

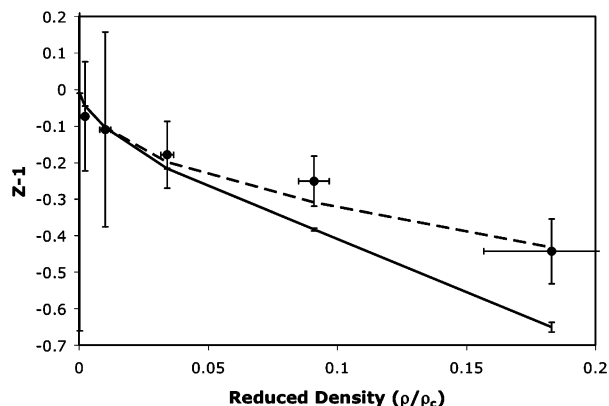


Figure 3. Deviation from ideality along the saturated vapor line of SPC water. Solid line is VEOS6, dashed line is VEOS5, and points are molecular simulation data from Vorholz et al.³⁹

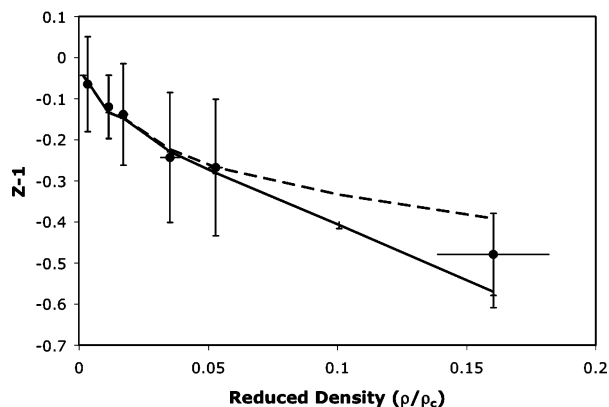


Figure 4. Deviation from ideality along the saturated vapor line of SPC/E water. Solid line is VEOS6, dashed line is VEOS5, and points are molecular simulation data from Boulougouris et al.²³

should be noted that we do not compute the saturated vapor line by itself from the virial coefficients obtained from Mayer sampling. Rather, we use known values of the saturation density and temperature of the model to define a coordinate to conduct the comparison. This locus of states represents the maximum density for which the vapor EOS may be of interest below the critical temperature.

We focus first on predicting PVT behavior along the saturated vapor line. Figures 3–6 show plots of $(Z - 1)$ [the deviation from ideality] versus reduced density ($\rho_r = \rho/\rho_c$, where ρ_c is the critical density of the model) along the saturated vapor line for four of the five water models studied: SPC, SPC/E, MSPC/E, and TIP4P. In each figure, the points represent molecular simulation data (complete with error bars calculated from the reported uncertainties in pressure and density according to each investigation) from the literature, and the dashed and solid lines represent fifth- and sixth-order truncated virial series predictions, respectively. Again, it is important to mention here that we do not have Mayer sampling results for B_2 – B_6 for all the water models at all of the temperatures from the molecular simulation data. Therefore, to obtain values for the virial coefficients from the various water models at the desired temperatures, we interpolate using first-, second-, or third-order polynomial curves between successive data points, depending on the order of the coefficient.

Last, we must address the issue of the uncertainty associated with the VEOS5 and VEOS6 predictions for $(Z - 1)$. The overall uncertainty for each of these points was calculated via

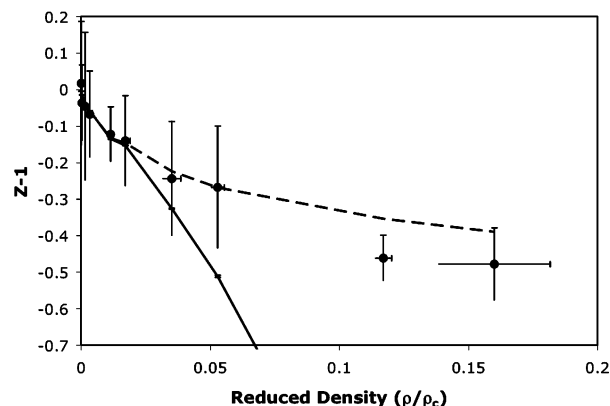


Figure 5. Deviation from ideality along the saturated vapor line of MSPC/E water. Solid line is VEOS6, dashed line is VEOS5, and points are molecular simulation data from Boulougouris et al.²³

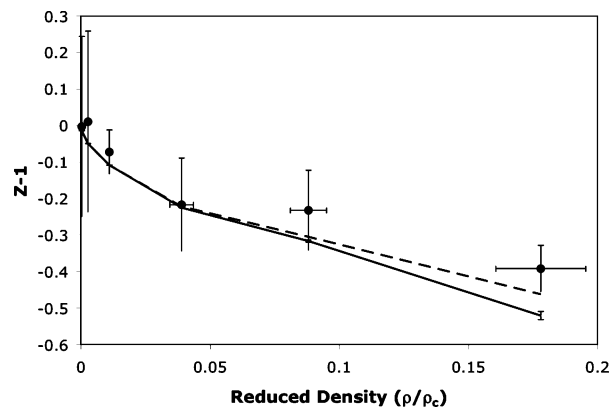


Figure 6. Deviation from ideality along the saturated vapor line of TIP4P water. Solid line is VEOS6, dashed line is VEOS5, and points are molecular simulation data from Vorholz et al.³⁹

propagation of error on the virial coefficients, taking the uncertainty for each virial coefficient at the temperature of interest to be equal to the maximum absolute uncertainty of the two coefficient values at the temperatures closest to it (see Tables 2–6, accordingly).

In general, for all four water models, the fifth-order truncated virial series (VEOS5) is better at matching the saturated vapor data than the sixth-order truncated virial series (VEOS6). At all state points for all water models, VEOS6 predicts too great a deviation from ideal gas behavior. Despite this commonality, there are some notable differences and features between VEOS5 and VEOS6 for the various water models. These include

- For SPC water, VEOS6 begins to deviate significantly from the simulation results at a reduced density of ~ 0.09 , whereas VEOS5 performs exceptionally well out to reduced densities of 0.18. It should be noted that the highest reduced density point at which VEOS5 agrees with simulation data for SPC water in Figure 3 corresponds to a reduced temperature of 0.93. It is very interesting to see how well VEOS5 captures PVT behavior for so long along the saturated vapor line, approaching the critical point.

- In the case of SPC/E water, both virial series agree with simulation data, within uncertainty, up to a ρ_r of ~ 0.16 . Beyond that density, both series begin to fail, with VEOS6 diverging faster from the simulated saturated vapor line than VEOS5.

- VEOS6 for MSPC/E water, as shown in Figure 5, fails at much lower reduced densities than the sixth-order equations for SPC and SPC/E.

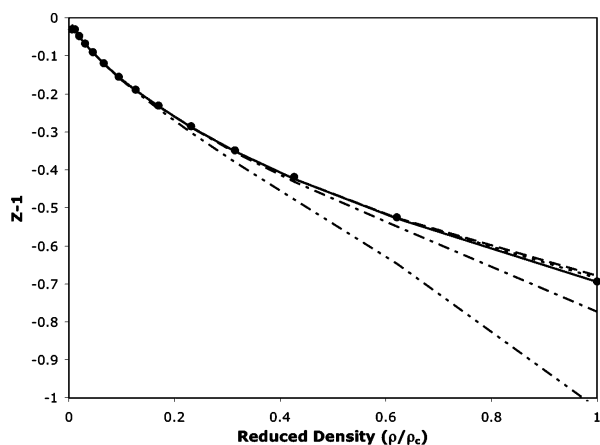


Figure 7. Deviation from ideality along the saturated vapor line of the Lennard-Jones model. — VEOS6, - - - VEOS5, VEOS4, - · - · VEOS3, - · · - · VEOS2. Points are molecular simulation data from Lofti et al.⁴⁰

• For TIP4P water, the difference between VEOS5 and VEOS6 predictions is rather small. This indicates that the importance of higher-order coefficients is specific to the water model under consideration.

It is worthwhile to pause and comment on the notion of “accuracy” when comparing VEOS5 and VEOS6 predictions to molecular simulation data. In one sense, VEOS5 is more “accurate” than VEOS6 in matching the simulation saturated vapor line; that is, it does a better job of predicting the correct pressure (and therefore, the compressibility factor, Z) given a specific temperature and density. However, in the purest sense, VEOS6 is inherently more “accurate” than VEOS5 on the basis of the fact that it includes B_6 , a term which does belong in the virial series and whose value can be determined with reasonable precision via Mayer sampling. Therefore, the fact that VEOS5 matches the saturated vapor line better is likely fortuitous, a result that probably stems from omitting higher-order terms that normally would cancel each other out at the given thermodynamic state points along the saturated vapor line. In this sense, Figures 3–6 actually test the ability of a fifth-order truncated series to reproduce the saturated vapor line. Once VEOS6 begins to deviate significantly from VEOS5, one can know with certainty that truncation at B_5 is no longer appropriate. Further, the fact that VEOS6, which is inherently more “accurate” given its inclusion of B_6 , deviates significantly (more than can be ascribed to imprecision in B_6) from the simulation data indicates that B_7 (at least) is required to better reproduce the PVT behavior along the saturated vapor line. Alternatively, it is also possible that the virial series is not convergent at the conditions being studied here. We would not have expected this, given that a similar study applied to the LJ fluid²⁰ shows increasing accuracy with added coefficients (up to B_6) along the saturation curve (see Figure 7). Some indication of the difference in the convergence behavior is apparent in the critical-scaled plots of the coefficients presented in Figure 1, where the water coefficients are seen to greatly exceed the magnitude of the LJ coefficients. It is not clear whether the extra difficulty with water is due to its long-ranged interactions or strong short-ranged interactions. Some preliminary results (not reported here) for low-order coefficients for polarizable water models indicate that this behavior may be an artifact of the condensed-phase parametrization of these pairwise water models.

In addition to exploring PVT properties at subcritical temperatures (corresponding to the saturated vapor line), we also explored properties at supercritical temperatures. Guissani and

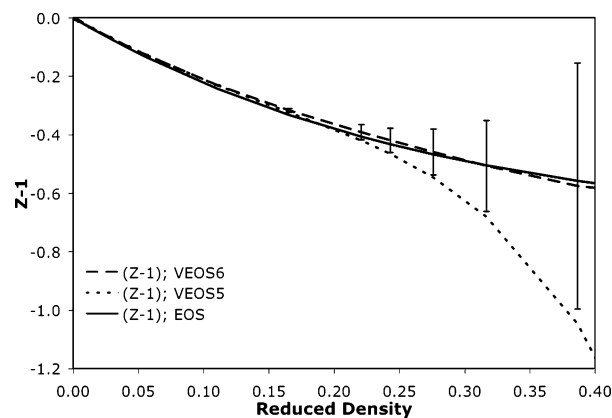


Figure 8. Deviation from ideality at $T_r = 1.03$ for SPC/E water. Solid line is EOS prediction of Guissani and Guillot,³⁷ dashed line is VEOS6, and dotted line is VEOS5. Error bars are shown for VEOS6 predictions.

Guillot performed a molecular dynamics study of SPC/E water and fit their simulation data to an empirical expression for the compressibility factor.³⁷ This expression (hereafter referred to as GGEOS) is valid for temperatures between 500 and 700 K and can be used as a standard for the PVT behavior of SPC/E water. Figure 8 compares $(Z - 1)$ versus ρ_r for VEOS5 and VEOS6 with the GGEOS at a reduced temperature of 1.03 (673 K for SPC/E water). From this plot, one notes that at this supercritical temperature, VEOS6 outperforms VEOS5, notwithstanding the relatively large confidence limits associated with VEOS6 predictions. VEOS5 begins to fail around $\rho_r \approx 0.25$, whereas VEOS6 accurately reproduces the behavior of the GGEOS out to $\rho_r = 0.40$. This figure highlights the importance of higher-order virial coefficients such as B_6 in successfully quantifying the thermodynamics of denser, gas-like, near-critical and supercritical water. Last, it should be noted that the high uncertainty in the VEOS6 predictions is dominated by the relatively high uncertainty in B_6 for SPC/E at 673 K (see Table 2). Here, one notes that for $\rho_r > 0.2$ the overall uncertainty in VEOS6 grows rapidly as ρ_r increases, owing largely to the effect of multiplying larger densities by the more imprecise value for B_6 .

Kalinichev and Churakov explored the PVT properties of supercritical TIP4P water.⁴¹ They performed molecular dynamics simulations at three temperatures: 623, 673, and 773 K, which correspond to reduced temperatures of 1.04, 1.12, and 1.29, respectively. From inspection of Table 6, one notes that we do not have simulation results for B_2 – B_6 for TIP4P at these three temperatures. Therefore, to obtain values for the virial coefficients at these three temperatures, we interpolate as was described for saturated vapor conditions. Figure 9 presents $(Z - 1)$ versus ρ_r for both VEOS5 and VEOS6 for TIP4P water and compares them to simulation data for the three temperatures of interest. From the figure, one notes that for reduced temperatures of 1.04 and 1.29, VEOS5 is only slightly more accurate than VEOS6. However, at $T_r = 1.12$, VEOS6 appears to reproduce the simulation data better out to larger reduced densities (~ 0.32).

3.1.2. Joule–Thomson Coefficient at Zero Pressure. An additional thermodynamic property of interest is u^0 , the Joule–Thomson (J – T) coefficient at zero pressure. This coefficient, as a function of temperature, is often used to estimate the second virial coefficient. It can be used further to parametrize an intermolecular potential for a particular species under investigation. In addition, J – T coefficients give insight into inversion temperatures, which are important for throttling processes.⁴²

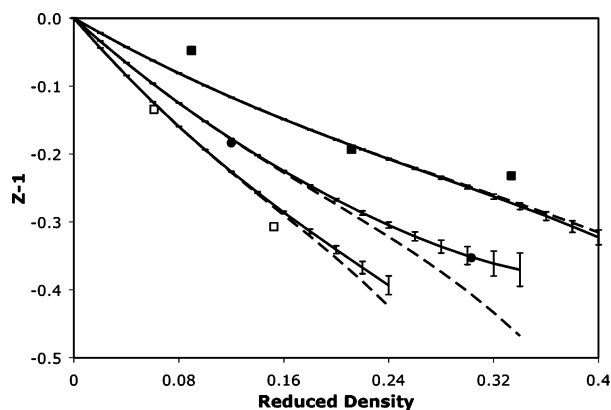


Figure 9. Deviation from ideality for supercritical TIP4P water. Solid lines are VEOS6, dashed lines are VEOS5, and points are molecular simulation data from Kalinichev and Churakov:⁴¹ □ $T_r = 1.04$, ● $T_r = 1.12$, and ■ $T_r = 1.29$.

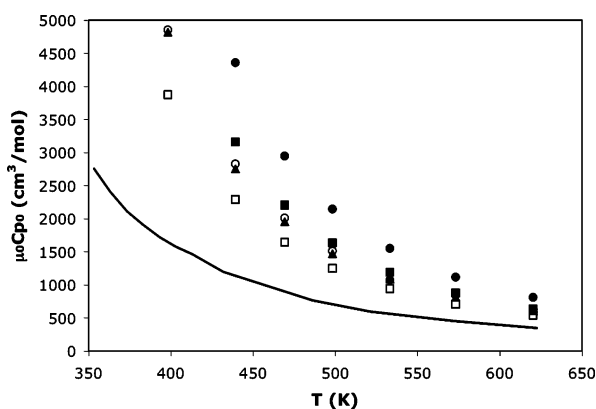


Figure 10. Joule–Thomson coefficients for various virial equations of state. Solid line is experimental values,^{44,45} and points correspond to the following water models: ● SPC/E, ■ MSPC/E, ▲ SPC, ○ TIP3P, and □ TIP4P.

The J – T coefficient at zero pressure is given by¹¹

$$-\phi^0 \equiv \mu^0 C_p^0 = T \frac{dB_2}{dT} - B_2 \quad (11)$$

where C_p^0 is the zero-pressure value of the molar heat capacity. Rowlinson⁴³ reports the earliest calculation of J – T coefficients for water at zero pressure. Here, we report values of $(-\phi^0)$ for all the models used in this study and compare them with the available experimental data^{44,45} in Figure 10. To determine the value of dB_2/dT from the Mayer sampling results, we take derivatives of our polynomial-based interpolation functions for $B_2(T)$, as described in Section 3.1.1. As the figure shows, all of the water models predict the correct qualitative behavior as a function of temperature; however, all of the models overpredict the magnitude of $-\phi^0$. The TIP4P model does the best job of matching the experimental data. It should be noted that the TIP4P model, given its smaller predictions for $-\phi^0$, will predict a smaller inversion temperature than the other models. Additionally, it should be noted that the omission of quantum effects on the values of B_2 for the pairwise models studied here also contributes to the lack of agreement with real water, especially at lower temperatures.

4. Conclusion

Mayer sampling molecular simulation is used to determine values for B_2 – B_6 for SPC, SPC/E, MSPC/E, TIP3P, and TIP4P

water models. These virial coefficients are then used in virial series to predict PVT properties of saturated vapor-phase water and supercritical water, as well as Joule–Thomson coefficients. When scaled by the critical properties, the coefficients for water are much larger in magnitude than those previously calculated for the LJ model. The virial series up to B_6 behaves well at supercritical temperatures, but at subcritical conditions, the series does not show evidence of convergence at saturated-vapor densities. It is unclear whether the failure of the series including B_6 indicates that simply more coefficients are required or that the series is not convergent at these conditions.

Acknowledgment. Funding for this research was provided by Grant CTS-0414439 from the U.S. National Science Foundation. Some computations were performed on facilities provided by the University at Buffalo Center for Computational Research.

References and Notes

- (1) van der Waals, J. D. Thesis, Leiden, 1873.
- (2) McQuarrie, D. A. *Statistical Mechanics*; University Science Books: Sausalito, CA, 2000.
- (3) Reid, R. C.; Prausnitz, J. M.; Poling, B. E. *The Properties of Gases and Liquids*, 4th ed.; McGraw-Hill: Boston, MA, 1987.
- (4) Mason, E. A.; Spurling, T. H. The Virial Equation of State. *The International Encyclopedia of Physical Chemistry and Chemical Physics*; Topic 10: The Fluid State; Pergamon Press Ltd.: Oxford, 1969; Vol. 2.
- (5) Carnahan, N. F.; Starling, K. E. *J. Chem. Phys.* **1969**, *51*, 635.
- (6) Sanchez, I. C. *J. Chem. Phys.* **1994**, *101*, 7003.
- (7) Boublik, T. *Fluid Phase Equilib.* **2001**, *182*, 47.
- (8) Tomberli, B.; Goldman, S.; Gray, C. G. *Fluid Phase Equilib.* **2001**, *187*, 111.
- (9) Kusalik, P. G.; Liden, F.; Svishchev, I. M. *J. Chem. Phys.* **1995**, *103*, 10169.
- (10) MacDowell, L. G.; Menduina, C.; Vega, C.; de Miguel, E. *J. Chem. Phys.* **2003**, *119*, 11367.
- (11) Hirschfelder, J. O.; Curtiss, C. F.; Bird, R. B. *Molecular Theory of Gases and Liquids*; John Wiley & Sons: New York, 1954.
- (12) Woolley, H. W. *J. Chem. Phys.* **1953**, *21*, 236.
- (13) Benjamin, K. M.; Schultz, A. J.; Kofke, D. A. *Ind. Eng. Chem. Res.* **2006**, *45*, 5566.
- (14) Clisby, N.; McCoy, B. M. *J. Stat. Phys.* **2006**, *122*, 15.
- (15) Bishop, M.; Masters, A.; Vlasov, A. Y. *J. Chem. Phys.* **2005**, *122*, 154502.
- (16) Vlasov, A. Y.; You, X. M.; Masters, A. J. *Mol. Phys.* **2002**, *100*, 3313.
- (17) Sun, T.; Teja, A. S. *J. Phys. Chem.* **1996**, *100*, 17365.
- (18) Ree, F. H.; Hoover, W. G. *J. Chem. Phys.* **1964**, *40*, 939.
- (19) Rouha, M.; Nezbeda, I. *J. Mol. Liq.* **2007**, *134*, 107.
- (20) Singh, J. K.; Kofke, D. A. *Phys. Rev. Lett.* **2004**, *92*, 220601; **2005**, *94*, 249903 (erratum).
- (21) Berendsen, H. J. C.; Postma, J. P. M.; van Gunsteren, W. F.; Hermans, J. In *Intermolecular Forces*; Pullmann, B. Ed.; D. Reidel: Dordrecht, The Netherlands, 1981; p 331.
- (22) Berendsen, H. J. C.; Grigera, J. R.; Straatsma, T. P. *J. Phys. Chem.* **1987**, *91*, 6269.
- (23) Boulougouris, G. C.; Economou, I. G.; Theodorou, D. N. *J. Phys. Chem. B* **1998**, *102*, 1029.
- (24) Jorgensen, W. L.; Chandrasekhar, J.; Madura, J. D.; Impey, R. W.; Klein, M. L. *J. Chem. Phys.* **1983**, *79*, 926.
- (25) Jorgensen, W. L.; Madura, J. D. *Mol. Phys.* **1985**, *56*, 1381–1392.
- (26) Schenter, G. K. *J. Chem. Phys.* **2002**, *117*, 6573. Millot, C.; Soetens, J.-C.; Costa, M. T. C. M.; Hodges, M. P.; Stone, A. J. *J. Phys. Chem. A* **1998**, *102*, 754.
- (27) Rast, S.; Fries, P. H.; Krienke, H. *Mol. Phys.* **1999**, *96*, 1543.
- (28) Labik, S.; Gabrielova, H.; Kolafa, J.; Malijevsky, A. *Mol. Phys.* **2003**, *101*, 1139.
- (29) Phillips, P. W.; LaViolette, R. A.; Pratt, L. R. *J. Chem. Phys.* **1984**, *80*, 1605.
- (30) LaViolette, R. A.; Pratt, L. R. *Phys. Rev. A: At., Mol., Opt. Phys.* **1983**, *28*, 2482.
- (31) In this sense, Mayer sampling utilizes a different “base unit” for sampling from that found in conventional free energy perturbation applications; that is, the ratio of averages $\langle \gamma/\pi \rangle_\pi / \langle \gamma/\pi \rangle_\pi$ appears as the elementary perturbation, and multistage methods are built from it. This is necessary because the integrand of the desired configurational integral in Mayer sampling can have negative values.
- (32) Kofke, D. A. *Fluid Phase Equilib.* **2005**, *228*–229C, 41.

- (33) Kofke, D. A.; Frenkel, D. In *Handbook of Molecular Modeling*; Yip, S. Ed.; Springer: Dordrecht, The Netherlands, 2005; p 683.
- (34) Kofke, D. A.; Mihalick, B. C. *Fluid Phase Equilib.* **2002**, *194*, 327.
- (35) Bennett, C. H. *J. Comput. Phys.* **1976**, *22*, 245.
- (36) Frenkel, D.; Smit B. *Understanding Molecular Simulation: From Algorithms to Applications*; Academic Press: San Diego, CA, 1996.
- (37) Guissani, Y.; Guillot, B. *J. Chem. Phys.* **1993**, *98*, 8221.
- (38) Harvey, A. H.; Lemmon, E. W. *J. Phys. Chem. Ref. Data* **2004**, *33*, 369.
- (39) Vorholz, J.; Harismiadis, V. I.; Rumpf, B.; Panagiotopoulos, A. Z.; Maurer, G. *Fluid Phase Equilib.* **2000**, *170*, 203.
- (40) Lofti, A.; Vrabc, J.; Fischer, J. *Mol. Phys.* **1992**, *76*, 1319.
- (41) Kalinichev, A. G.; Churakov, S. V. *Fluid Phase Equilib.* **2001**, *183–184*, 271.
- (42) Smith, J. M.; Van Ness, H. C. *Introduction to Chemical Engineering Thermodynamics*, 4th ed.; McGraw-Hill: New York, 1987.
- (43) Rowlinson J. S. Doctoral Dissertation, Oxford, 1950.
- (44) McGlashan, M. L.; Wormald, C. J. *Chem. Thermodyn.* **2000**, *32*, 1489.
- (45) Ertle S. Doctoral Dissertation, Technische Universität München, Germany, 1979.
- (46) Johnson, J. K.; Zollweg, J. A.; Gubbins, K. E. *Mol. Phys.* **1993**, *78*, 591.